

Spacer-induced Forward Osmosis Membrane Integrity Loss during Gypsum Scaling

Desalination

Revised: April 2016

Ming Xie^{1*}, Chuyang Y. Tang² and Stephen R. Gray¹

¹ Institute for Sustainability and Innovation, College of Engineering and Science, Victoria University, PO Box 14428, Melbourne, Victoria 8001, Australia

² Department of Civil Engineering, The University of Hong Kong, Hong Kong

* Corresponding author: M.X., email: ming.xie@vu.edu.au; phone: +61 3 9919 8174

1 **ABSTRACT**

2 We demonstrated forward osmosis (FO) membrane integrity loss during gypsum scaling
3 with the presence of membrane spacer. The gypsum scalant had preferential accumulation
4 adjacent to membrane spacer where the needle-shape gypsum potentially compromised
5 polyamide thin-film composite FO membrane integrity. However, the loss of FO membrane
6 integrity cannot be sensitively detected by *in situ* measurements of membrane water and salt
7 (NaCl) permeability coefficients. We, for the first time, employed membrane integrity challenge
8 tests to reveal the impaired FO membrane integrity by fluorescent Rhodamine WT tracer and
9 amine-modified latex nanoparticles, respectively. Challenge tests using Rhodamine WT tracer
10 showed that membrane log removal value decreased to 3.5 after three scaling-cleaning cycles,
11 which corresponded to a pinhole size of 0.06 μm^2 on the FO membrane surface. This result was
12 further corroborated by challenge tests using latex nanoparticle where the particle size
13 distribution in the permeate became wider and the average particle size increased over the three
14 scaling-cleaning cycles. Both challenge tests were sensitive enough to identify impaired FO
15 membrane integrity. Results reported here have significant implications for achieving better
16 membrane spacer and module design, as well as demanding periodical monitoring of FO
17 membrane integrity in water reuse.

18

19 **Key words:** Forward osmosis; gypsum scaling; membrane integrity; fluorescent Rhodamine WT
20 tracer; amine-modified latex nanoparticle

21 1. Introduction

22 Membrane technologies respond to the global challenge for adequate and safe water [1,
23 2]. Forward osmosis (FO), an emerging osmosis-driven membrane process, has the potential to
24 advance seawater desalination and wastewater reuse [3]. Because of the low fouling propensity
25 and high fouling reversibility with simple membrane flushing, FO has potential applications in
26 treatment of a variety of high fouling potential source waters [4-7], including desalination of
27 high salinity brines from shale gas produced water [8-11], municipal wastewater reclamation
28 [12-16], and valuable resource recovery [17-19].

29 These challenging waste streams with complex foulants stress membrane mechanical
30 properties and subsequent membrane performance. For instance, recent studies reported minor
31 changes in FO membrane properties and performance after exposure to oil and gas wastewaters
32 [20]. More importantly, damage to FO membrane active layer was visualized after gypsum
33 scaling with the presence of membrane spacers [21]. These prior findings warrant a close
34 examination of FO membrane integrity during processing of wastewaters with high fouling
35 propensity.

36 Varying techniques were proposed to examine reverse osmosis (RO) membrane integrity,
37 such as fluorescent spectroscopy [22-24], Rutherford backscattering spectrometry [25, 26], and
38 flow cytometry [27]. For instance, fluorescence signatures, such as peak C as $\lambda_{Ex/Em} =$
39 3000/400 nm, were proposed to monitor RO membrane integrity due to relatively low noise and
40 variability of these fluorescent organic molecules [22]. For biological particles, such as virus,
41 flow cytometry demonstrated good sensitivity and reproducibility for quantifying virus reduction
42 rate along the treatment processes, which provide direct evidence for RO membrane integrity
43 monitoring [27].

44 These techniques aim to ensure that RO membrane achieves high log removal value
45 (LRV) for virus removal so as to address public health protection concerns, as well as regulatory
46 requirements. However, to date, there is no existing study that examines membrane integrity of
47 FO process, particularly in treatment of high fouling wastewaters. Such fundamental
48 understanding can lead to the development of monitoring techniques for FO membrane integrity,
49 which will significantly increase the efficiency and robustness of FO process.

50 In this study, we demonstrate that FO membrane integrity was compromised during
51 gypsum scaling. Membrane gypsum scaling was visualized by a real-time observation system.
52 Membrane integrity of three scaling-cleaning cycles was examined using challenge tests
53 comprising sensitive fluorescent Rhodamine WT tracer and amine-modified latex nanoparticles.
54

55 **2. Materials and methods**

56 *2.1 Real-time FO observation system*

57 A transparent, acrylic FO membrane cell coupled with microscopic observation enabled
58 real-time observation of gypsum scaling (Figure S1, Supplementary Data). Specifically, a
59 membrane coupon with an effective area of 20.2 cm² was placed in a transparent FO membrane
60 cell. A crossflow rate of 1 L/min (corresponding to crossflow velocity of 9 cm/s) was maintained
61 for both the feed and draw solutions using micro gear pumps. The FO water flux was determined
62 by measuring the weight changes of the feed solution at specific time intervals with a precision
63 balance connected to a computer and a data logging system.

64 Real-time membrane surface images of 2048 × 1536 pixels resolution were recorded using
65 a high resolution digital camera and an optical microscope (20× magnification). To minimize the
66 interference from air bubbles, the feed and draw solutions were degassed prior to circulation in
67 the FO setup. Through the combination of optical magnification along with a unique
68 combination of bright and low angle dark field illumination, provided by ultra-bright fiber optic
69 illuminator, digital image capture and analysis, occurrence and subtle changes of gypsum crystal
70 could be effectively monitored.

71 *2.2 Membrane and spacer*

72 A polyamide thin-film composite (TFC) forward osmosis (FO) membrane was employed
73 in this study. The TFC membrane was made of a thin selective polyamide active layer on top of a
74 porous polysulfone support layer [28].

75 Spacers are essential to an FO membrane module to maintain flow channel and provide
76 hydrodynamic conditions. Diamond-patterned, polypropylene spacers (65 mil (1.651 mm) spacer,
77 GE Osmonics), [which were also the current standard RO membrane spacer](#), were placed in both
78 the feed and draw channels during the experiments.

79 *2.3 Experimental protocol for gypsum scaling and cleaning*

80 A total of three gypsum scaling-cleaning cycles were conducted. The protocol for gypsum
81 scaling experiments comprised the following steps. First, a new membrane coupon, with the
82 active layer facing the feed solution, was placed in the membrane cell before each experiment
83 and stabilized to obtain a constant flux. The membrane in the FO mode (i.e., membrane active
84 layer faces feed solution) was stabilized with deionized water feed and 2 M NaCl draw. Next, the
85 gypsum scaling experiment was performed for about 24 h to obtain approximately 1400 mL
86 cumulative permeate volume at the conclusion of each experiment. The gypsum scaling solution
87 was comprised of 35 mM CaCl₂, 20mM Na₂SO₄, and 19 mM NaCl, with a gypsum
88 (CaSO₄·2H₂O) saturation index (SI) of 1.3. Other experimental conditions were: crossflow
89 velocity of 9 cm/s, ambient pH (pH 6.8), and temperature of 25.0 ± 0.1°C. Water flux was
90 continuously monitored throughout the fouling experiments by a data logger. A baseline
91 experiment (i.e., feed without CaCl₂ and Na₂SO₄) was also carried out to correct the flux decline
92 due to the continuous concentration of the feed solution and dilution of the draw solution, as
93 described in our previous publication [7]. The real-time monitoring system captured images of
94 the FO membrane surface every 30 minutes during the scaling experiment to identify the
95 occurrence and development of gypsum crystals on FO membrane surface during scaling
96 experiment.

97 Membrane cleaning was performed immediately after the FO scaling experiments.
98 Deionized water flushing was carried out in both feed and draw flow channels at 18 cm/s for
99 30 min. The membrane water flux after cleaning was measured using deionized water feed and 2
100 M NaCl draw.

101 Key membrane transport parameters (water permeability coefficients, A and salt (NaCl)
102 permeability coefficient, B) of pristine membrane and membrane after each cycle were
103 determined according to a method previously described [29]. Briefly, the determination of key
104 membrane transport parameters comprises a single FO experiment divided into four stages, each
105 using a different concentration of draw solution. The experimental water and reverse salt fluxes
106 measured in each stage are fitted to the corresponding FO transport equations by performing a
107 least-squares non-linear regression, using A , B , and S as regression parameters. Four different
108 NaCl draw concentrations (approximately 0.2, 0.4, 0.7, and 1.2 M NaCl) were employed. These
109 parameters were adjusted to fit the experimental data of water and reverse salt fluxes to the
110 corresponding governing equations. This method allowed an *in situ* measurement of membrane
111 characteristics *without* taking the FO membrane out of the membrane cell and transferring into a
112 pressurized RO filtration setup, which could potentially impair membrane integrity.

113 2.4 FO membrane integrity examination

114 Apart from measuring key membrane transport parameters, FO membrane integrity at the
115 conclusion of each gypsum scaling-cleaning cycle was examined by challenge tests using two
116 tracers: fluorescent Rhodamine WT (Tuner Designs, CA, USA) and amine-modified polystyrene
117 latex nanoparticle (Sigma-Aldrich, MO, USA), respectively. Details regarding these two tracers
118 were provided in the Supplementary Data (Table S1). Specifically, the challenge tests were
119 conducted in single-pass mode where neither feed nor draw solution were returned to their
120 reservoirs. A pulse of either fluorescent Rhodamine WT solution of 50 mg/L or amine-modified
121 polystyrene latex nanoparticle solution of 20 mg/L was injected into the FO feeding tube for 60
122 seconds at a crossflow rate of 1 L/min (corresponding to crossflow velocity of 9 cm/s). At the
123 same time, the draw solution at a crossflow rate of 1 L/min (corresponding to crossflow velocity
124 of 9 cm/s) was sampled every 10 seconds for a total of 540 seconds to generate either a time-
125 concentration profile of fluorescent Rhodamine WT or the nanoparticle size distribution in the
126 draw solution. A detailed description of challenge tests is provided in the supplementary
127 materials and methods, Supplementary Data. Concentration of fluorescent Rhodamine WT was
128 quantified by a fluorometer (AquaFluor, Tuner Design, CA, USA) at excitation wavelength of
129 530 nm and emission wavelength of 555 nm. Nanoparticle size distribution was determined by
130 dynamic light scattering (Zetasizer Nano ZSP, Malvern Instruments, Worcestershire, UK).

131 The log removal value (LRV) of fluorescent Rhodamine WT was calibrated as a function
132 of pinhole size in order to quantify the degree of FO membrane integrity loss. The FO membrane
133 integrity loss was artificially induced by lightly tapping the membrane samples using a tip of a
134 hypodermic needle (GL Sciences, Tokyo, Japan). Pinholes of various sizes ($0.02\text{-}0.08\ \mu\text{m}^2$) were
135 created on the FO membrane sample that was subjected to the aforementioned fluorescent
136 Rhodamine WT challenge test. The LRV value was calculated by:

$$137 \quad LRV = \log\left(\frac{C_{draw} DF}{C_{feed}}\right) \quad (1)$$

138 where C_{draw} was the Rhodamine WT trace concentration in the draw; DF was the dilution factor
139 of Rhodamine WT trace by considering the draw solution volume; C_{feed} was the Rhodamine WT
140 trace concentration in the feed. It was assumed that the feed Rhodamine WT trace concentration
141 remained constant during the short period of challenge test.

142

143 **3. Results and Discussion**

144 *3.1 Gypsum scalant accumulates adjacent to spacer filament*

145 Membrane spacer significantly affected membrane performance and gypsum scaling
146 pattern. Membrane spacer not only alleviated gypsum scaling (Figure 1A), but also induced
147 preferential accumulation of gypsum scalant adjacent to spacer filament (Figure 1B). Specifically,
148 membrane spacer abated water flux decline by 22% during gypsum scaling in comparison with
149 FO filtration without membrane spacer. The enhanced membrane performance was attributed to
150 the mitigation of concentration polarization at membrane interface by membrane spacer [30-32].

151 **[Figure 1]**

152 More importantly, real-time microscopic observation demonstrated that gypsum scaling
153 was initiated next to spacer filament, and progressively resulted in severe accumulation of
154 gypsum scalant in the confined region close to spacer filament (Figure 1B, and Video S1,
155 Supplementary Data). [In comparison with the gypsum scaling without membrane spacer \(Figure](#)
156 [S4, Supplementary Data\), our real-time microscopic imaging showed that gypsum scalant](#)
157 [preferentially accumulated adjacent to the membrane spacers.](#) Such gypsum scaling pattern was
158 mainly driven by the hydrodynamic dead zones created near the filaments, thereby favoring the

159 crystallization and growth of gypsum scalant. Our results also agreed well with prior studies of
160 particulate scaling in FO process, using latex particle [33] and microalgae [34], which
161 preferentially accumulated at regions next to the fabric filaments in the filtration. These
162 observations were consistent with previous knowledge of RO scaling [35-37], that crystal
163 formation and precipitate deposition occurred preferentially at the spacer induced hydrodynamic
164 dead zones.

165 SEM micrographs of the gypsum-scaled membrane further verified the preferential
166 accumulation of gypsum scalant adjacent to membrane spacers (Figure 2). More importantly,
167 these images also revealed the indentation and possible pinholes on the membrane active layer
168 after removing membrane spacers (Figures 2B and D). As a result, it raised concerns regarding
169 FO membrane integrity when needle-shaped gypsum crystal morphology was revealed in the
170 confined region adjacent to spacer filament (Figure 2). As a result, it was hypothesized that such
171 gypsum scaling pattern could potentially compromise FO membrane integrity, and further
172 evidence to support this hypothesis is provided in the following sections.

173 [Figure 2]

174 3.2 Membrane transport parameters measurements cannot identify membrane integrity loss

175 Key membrane transport parameters – water permeability coefficient, A , and salt (NaCl)
176 permeability coefficient, B – were measured *in situ* at the conclusion of each scaling-cleaning
177 cycle using a single FO experimental method [29]. This method minimized potential mechanical
178 damage of the FO membrane by undertaking the characterization *in situ*, rather than transforming
179 into and testing by a pressurized RO membrane cell.

180 Statistically, negligible differences in membrane A and B values were observed (Figure 3)
181 between pristine membrane and membranes after three scaling-cleaning cycles (student t -test, P
182 value > 0.05). Largely unchanged membrane water and salt (NaCl) permeabilities also agreed
183 with the high water flux recovery (>97%) after membrane physical flushing (Figure S3,
184 Supporting Information), which benefited from the high fouling reversibility of FO process [6,
185 38, 39]. However, limited variations in water and salt (NaCl) permeability coefficients were not
186 sufficiently sensitive to reflect the potential loss of membrane integrity. As a result, we employed
187 membrane integrity challenge tests comprising two tracers – fluorescent Rhodamine WT and

188 amine-modified polystyrene latex nanoparticles – to more closely examine membrane integrity
189 during gypsum scaling.

190 **[Figure 3]**

191 *3.3 Fluorescent dye tracer and latex nanoparticle challenge tests reveal membrane integrity loss.*

192 Membrane integrity challenge tests were performed by introducing a pulse of tracer that
193 enabled sensitive detection of breach of membrane integrity. Two tracers were used to examine
194 the loss of membrane integrity. First, fluorescent Rhodamine WT, which has been previously
195 used to monitor RO membrane integrity [40], can be detected at low concentration of $0.04 \mu\text{g L}^{-1}$
196 using the current analytical method. The intact FO membrane achieved LRV up to 5.1 using
197 fluorescent Rhodamine WT (Figure 4). Second, the amine-modified latex nanoparticles with
198 average particle size of 50 nm, which is equivalent to the size of virus, did not show severe
199 aggregation during of the challenge test (Figure S3, Supplementary Data), which making it an
200 excellent surrogate for FO membrane integrity for virus removal [25].

201 *3.3.1 Fluorescent Rhodamine WT challenge test*

202 Concentration-time profile of Rhodamine WT demonstrated a progressive increase of
203 Rhodamine WT concentration in the draw solution, which indicated a breach of membrane
204 integrity (Figure 4A). For instance, at the conclusion of the second scaling-cleaning cycle (Cycle
205 II), Rhodamine WT peak could be clearly identified with concentration of $6 \mu\text{g L}^{-1}$,
206 corresponding to an LRV of 4 [41]. More importantly, this 4 LRV credit of the FO membrane
207 was compromised after three gypsum scaling-cleaning cycles.

208 In order to provide insights into the degree of membrane integrity loss, we also correlated
209 the membrane LRV as a function of pinhole size to quantify the degree of membrane integrity
210 loss during the gypsum scaling (Figure 4B). The SEM images, showing the localization of
211 defects formation near the spacer filaments (Figure 2), cannot accurately reflect membrane
212 integrity loss during the gypsum scaling. Using the calibrated pinhole size-LRV curve (Figure
213 4B), we demonstrated that membrane integrity loss was equivalent to a membrane with pinhole
214 size of $0.065 \mu\text{m}^2$ (Figure 4B) when gypsum scalant accumulated adjacent to spacer filament at
215 the conclusion of three scaling-cleaning cycles.

216 **[Figure 4]**

247 Results reported here highlighted the FO membrane integrity loss using fluorescent
248 Rhodamin WT tracer and latex nanoparticle, during gypsum scaling with the presence of
249 membrane spacer. Such FO membrane integrity loss was driven by the preferential accumulation
250 of gypsum scalant adjacent to membrane spacer where the needle-shape gypsum potentially
251 compromised FO membrane integrity. More importantly, the routine measurements of FO
252 membrane water and salt (NaCl) permeabilities cannot identify the membrane integrity breach,
253 which warranted the employment of membrane integrity challenge tests by Rhodamine WT
254 tracer and amine-modified latex nanoparticles, respectively. As a result, challenge tests using
255 Rhodamine WT tracer showed that membrane log removal value decreased to 3.5 after three
256 scaling-cleaning cycles, which corresponded to a pinhole size of $0.06 \mu\text{m}^2$ on the FO membrane
257 surface. This result was further corroborated by challenge tests using latex nanoparticle where
258 the particle size distribution in the permeate became wider and the average particle size increased
259 over the three scaling-cleaning cycles. Both challenge tests were sensitive enough to identify
260 impaired FO membrane integrity. Results reported here have significant implications for
261 achieving better membrane spacer and module design, as well as demanding periodical
262 monitoring of FO membrane integrity in water reuse.

263 **3.6 Acknowledgements**

264 M.X. thanks the Victoria University for Vice Chancellor Early Career Research
265 Fellowship.

266 3.7 References

- 267 [1] M.A. Shannon, P.W. Bohn, M. Elimelech, J.G. Georgiadis, B.J. Marinas, A.M. Mayes,
268 Science and technology for water purification in the coming decades, *Nature*, 452 (2008) 301-
269 310.
- 270 [2] M. Elimelech, W.A. Phillip, The Future of Seawater Desalination: Energy, Technology, and
271 the Environment, *Science*, 333 (2011) 712-717.
- 272 [3] D.L. Shaffer, J.R. Werber, H. Jaramillo, S. Lin, M. Elimelech, Forward osmosis: Where are
273 we now?, *Desalination*, 356 (2015) 271-284.
- 274 [4] B. Mi, M. Elimelech, Organic fouling of forward osmosis membranes: Fouling reversibility
275 and cleaning without chemical reagents, *Journal of Membrane Science*, 348 (2010) 337-345.
- 276 [5] B. Mi, M. Elimelech, Chemical and physical aspects of organic fouling of forward osmosis
277 membranes, *Journal of Membrane Science*, 320 (2008) 292-302.
- 278 [6] M. Xie, L.D. Nghiem, W.E. Price, M. Elimelech, Impact of organic and colloidal fouling on
279 trace organic contaminant rejection by forward osmosis: Role of initial permeate flux,
280 *Desalination*, 336 (2014) 146-152.
- 281 [7] M. Xie, J. Lee, L.D. Nghiem, M. Elimelech, Role of pressure in organic fouling in forward
282 osmosis and reverse osmosis, *Journal of Membrane Science*, 493 (2015) 748-754.
- 283 [8] G. Chen, Z. Wang, L.D. Nghiem, X.-M. Li, M. Xie, B. Zhao, M. Zhang, J. Song, T. He,
284 Treatment of shale gas drilling flowback fluids (SGDFs) by forward osmosis: Membrane fouling
285 and mitigation, *Desalination*, 366 (2015) 113-120.
- 286 [9] D.L. Shaffer, L.H. Arias Chavez, M. Ben-Sasson, S. Romero-Vargas Castrillón, N.Y. Yip,
287 M. Elimelech, Desalination and Reuse of High-Salinity Shale Gas Produced Water: Drivers,
288 Technologies, and Future Directions, *Environmental Science & Technology*, 47 (2013) 9569-
289 9583.
- 290 [10] B.D. Coday, P. Xu, E.G. Beaudry, J. Herron, K. Lampi, N.T. Hancock, T.Y. Cath, The
291 sweet spot of forward osmosis: Treatment of produced water, drilling wastewater, and other
292 complex and difficult liquid streams, *Desalination*, 333 (2014) 23-35.
- 293 [11] B.D. Coday, N. Almaraz, T.Y. Cath, Forward osmosis desalination of oil and gas
294 wastewater: Impacts of membrane selection and operating conditions on process performance,
295 *Journal of Membrane Science*, 488 (2015) 40-55.
- 296 [12] A. Achilli, T.Y. Cath, E.A. Marchand, A.E. Childress, The forward osmosis membrane
297 bioreactor: A low fouling alternative to MBR processes, *Desalination*, 239 (2009) 10-21.
- 298 [13] R.W. Holloway, J. Regnery, L.D. Nghiem, T.Y. Cath, Removal of Trace Organic Chemicals
299 and Performance of a Novel Hybrid Ultrafiltration-Osmotic Membrane Bioreactor,
300 *Environmental Science & Technology*, 48 (2014) 10859-10868.
- 301 [14] J. Zhang, W.L.C. Loong, S. Chou, C. Tang, R. Wang, A.G. Fane, Membrane biofouling and
302 scaling in forward osmosis membrane bioreactor, *Journal of Membrane Science*, 403-404 (2012)
303 8-14.

- 304 [15] L. Chen, Y. Gu, C. Cao, J. Zhang, J.-W. Ng, C. Tang, Performance of a submerged
305 anaerobic membrane bioreactor with forward osmosis membrane for low-strength wastewater
306 treatment, *Water Research*, 50 (2014) 114-123.
- 307 [16] M. Xie, L.D. Nghiem, W.E. Price, M. Elimelech, A Forward Osmosis–Membrane
308 Distillation Hybrid Process for Direct Sewer Mining: System Performance and Limitations,
309 *Environmental Science & Technology*, 47 (2013) 13486-13493.
- 310 [17] M.S. Diallo, G. Baier, B.A. Moyer, B. Hamelers, Critical Materials Recovery from
311 Solutions and Wastes: Retrospective and Outlook, *Environmental Science & Technology*, 49
312 (2015) 9387-9389.
- 313 [18] J. Zhang, Q. She, V.W.C. Chang, C.Y. Tang, R.D. Webster, Mining Nutrients (N, K, P)
314 from Urban Source-Separated Urine by Forward Osmosis Dewatering, *Environmental Science &*
315 *Technology*, 48 (2014) 3386-3394.
- 316 [19] M. Xie, L.D. Nghiem, W.E. Price, M. Elimelech, Toward Resource Recovery from
317 Wastewater: Extraction of Phosphorus from Digested Sludge Using a Hybrid Forward Osmosis–
318 Membrane Distillation Process, *Environmental Science & Technology Letters*, 1 (2014) 191-
319 195.
- 320 [20] B.D. Coday, C. Hoppe-Jones, D. Wandera, J. Shethji, J. Herron, K. Lampi, S.A. Snyder,
321 T.Y. Cath, Evaluation of the transport Parameters and physiochemical properties of forward
322 osmosis Membranes after treatment of produced water, *Journal of Membrane Science*.
- 323 [21] Y.-N. Wang, E. Järvelä, J. Wei, M. Zhang, H. Kyllönen, R. Wang, C.Y. Tang, Gypsum
324 scaling and membrane integrity of osmotically driven membranes: The effect of membrane
325 materials and operating conditions, *Desalination*, 377 (2016) 1-10.
- 326 [22] S. Singh, R.K. Henderson, A. Baker, R.M. Stuetz, S.J. Khan, Characterisation of reverse
327 osmosis permeates from municipal recycled water systems using fluorescence spectroscopy:
328 Implications for integrity monitoring, *Journal of Membrane Science*, 421–422 (2012) 180-189.
- 329 [23] M.-L. Pype, D. Patureau, N. Wery, Y. Poussade, W. Gernjak, Monitoring reverse osmosis
330 performance: Conductivity versus fluorescence excitation–emission matrix (EEM), *Journal of*
331 *Membrane Science*, 428 (2013) 205-211.
- 332 [24] M. Kumar, S. Adham, J. DeCarolis, Reverse osmosis integrity monitoring, *Desalination*,
333 214 (2007) 138-149.
- 334 [25] B. Mi, C.L. Eaton, J.-H. Kim, C.K. Colvin, J.C. Lozier, B.J. Mariñas, Removal of biological
335 and non-biological viral surrogates by spiral-wound reverse osmosis membrane elements with
336 intact and compromised integrity, *Water Research*, 38 (2004) 3821-3832.
- 337 [26] B. Mi, D.G. Cahill, B.J. Mariñas, Physico-chemical integrity of nanofiltration/reverse
338 osmosis membranes during characterization by Rutherford backscattering spectrometry, *Journal*
339 *of Membrane Science*, 291 (2007) 77-85.
- 340 [27] X. Huang, J.H. Min, W. Lu, K. Jaktar, C. Yu, S.C. Jiang, Evaluation of methods for reverse
341 osmosis membrane integrity monitoring for wastewater reuse, *Journal of Water Process*
342 *Engineering*, 7 (2015) 161-168.
- 343 [28] T.Y. Cath, M. Elimelech, J.R. McCutcheon, R.L. McGinnis, A. Achilli, D. Anastasio, A.R.
344 Brady, A.E. Childress, I.V. Farr, N.T. Hancock, J. Lampi, L.D. Nghiem, M. Xie, N.Y. Yip,

345 Standard Methodology for Evaluating Membrane Performance in Osmotically Driven Membrane
346 Processes, *Desalination*, 312 (2013) 31-38.

347 [29] A. Tiraferri, N.Y. Yip, A.P. Straub, S. Romero-Vargas Castrillon, M. Elimelech, A method
348 for the simultaneous determination of transport and structural parameters of forward osmosis
349 membranes, *Journal of Membrane Science*, 444 (2013) 523-538.

350 [30] M. Park, J.H. Kim, Numerical analysis of spacer impacts on forward osmosis membrane
351 process using concentration polarization index, *Journal of Membrane Science*, 427 (2013) 10-20.

352 [31] R. Valladares Linares, S.S. Bucs, Z. Li, M. AbuGhdeeb, G. Amy, J.S. Vrouwenvelder,
353 Impact of spacer thickness on biofouling in forward osmosis, *Water Research*, 57 (2014) 223-
354 233.

355 [32] H. Zhang, S. Cheng, F. Yang, Use of a spacer to mitigate concentration polarization during
356 forward osmosis process, *Desalination*, 347 (2014) 112-119.

357 [33] Y. Wang, F. Wicaksana, C.Y. Tang, A.G. Fane, Direct Microscopic Observation of Forward
358 Osmosis Membrane Fouling, *Environmental Science & Technology*, 44 (2010) 7102-7109.

359 [34] S. Zou, Y.-N. Wang, F. Wicaksana, T. Aung, P.C.Y. Wong, A.G. Fane, C.Y. Tang, Direct
360 microscopic observation of forward osmosis membrane fouling by microalgae: Critical flux and
361 the role of operational conditions, *Journal of Membrane Science*, 436 (2013) 174-185.

362 [35] G. An, J. Lin, J. Li, X. Li, X. Jian, Non-invasive measurement of membrane scaling and
363 cleaning in spiral-wound reverse osmosis modules by ultrasonic time-domain reflectometry with
364 sound intensity calculation, *Desalination*, 283 (2011) 3-9.

365 [36] G.Y. Chai, A.R. Greenberg, W.B. Krantz, Ultrasound, gravimetric, and SEM studies of
366 inorganic fouling in spiral-wound membrane modules, *Desalination*, 208 (2007) 277-293.

367 [37] A.I. Radu, L. Bergwerff, M.C.M. van Loosdrecht, C. Picioreanu, A two-dimensional
368 mechanistic model for scaling in spiral wound membrane systems, *Chemical Engineering*
369 *Journal*, 241 (2014) 77-91.

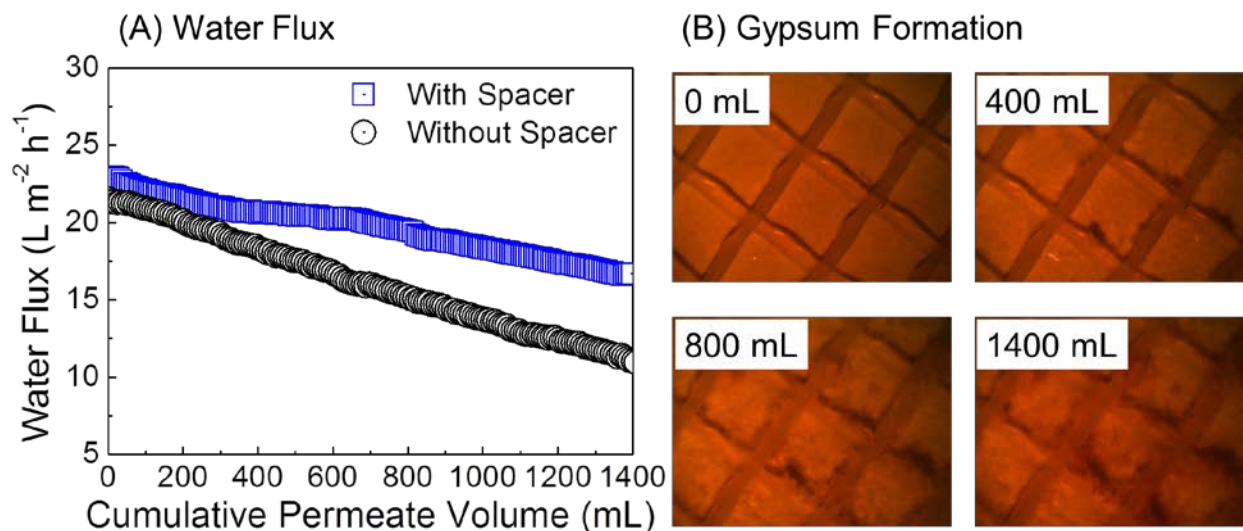
370 [38] M. Xie, L.D. Nghiem, W.E. Price, M. Elimelech, Impact of humic acid fouling on
371 membrane performance and transport of pharmaceutically active compounds in forward osmosis,
372 *Water Research*, 47 (2013) 4567-4575.

373 [39] M. Xie, M. Zheng, P. Cooper, W.E. Price, L.D. Nghiem, M. Elimelech, Osmotic dilution for
374 sustainable greenwall irrigation by liquid fertilizer: Performance and implications, *Journal of*
375 *Membrane Science*, 494 (2015) 32-38.

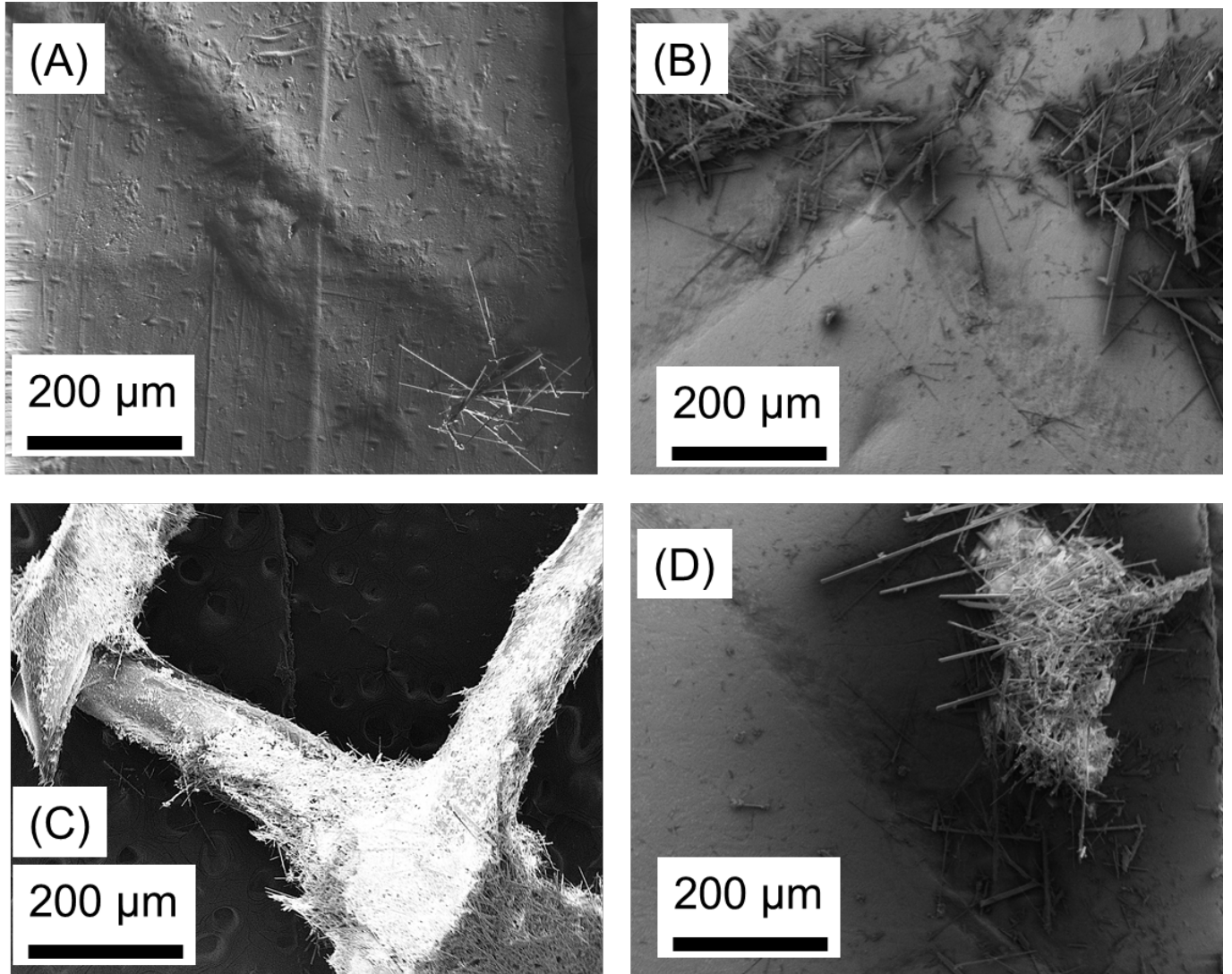
376 [40] S. Surawanvijit, J. Thompson, A. Rahardianto, V. Frenkel, Y. Cohen, Pulsed marker method
377 for real-time detection of reverse osmosis membrane integrity loss, *Desalination*, 370 (2015) 25-
378 32.

379 [41] L.F. Greenlee, D.F. Lawler, B.D. Freeman, B. Marrot, P. Moulin, Reverse osmosis
380 desalination: Water sources, technology, and today's challenges, *Water Research*, 43 (2009)
381 2317-2348.

382



383
 384 **Figure 1:** Gypsum scaling during forward osmosis filtration: (A) water flux decline as a function
 385 of cumulative permeate volume with and without membrane spacer; and (B) real-time
 386 microscopic observation at specific cumulative permeate volumes for experiments with spacer.
 387 Experimental conditions were: the scaling solution contains 35 mM CaCl₂, 20mM Na₂SO₄, and
 388 19 mM NaCl, with a gypsum saturation index of 1.3. A 2 M NaCl draw solution was used in FO.
 389 Diamond-patterned, polypropylene spacers (65 mil (1.651 mm)) were used in feed and draw
 390 solution sides, crossflow velocity of 9 cm/s, ambient pH (pH 6.8), and temperature of 25.0 ±
 391 0.1°C. Representative real-time images were taken at specific cumulative permeate volumes.
 392 Note that the flux for the fouled membrane is corrected by the initial flux in the fouling
 393 experiments.



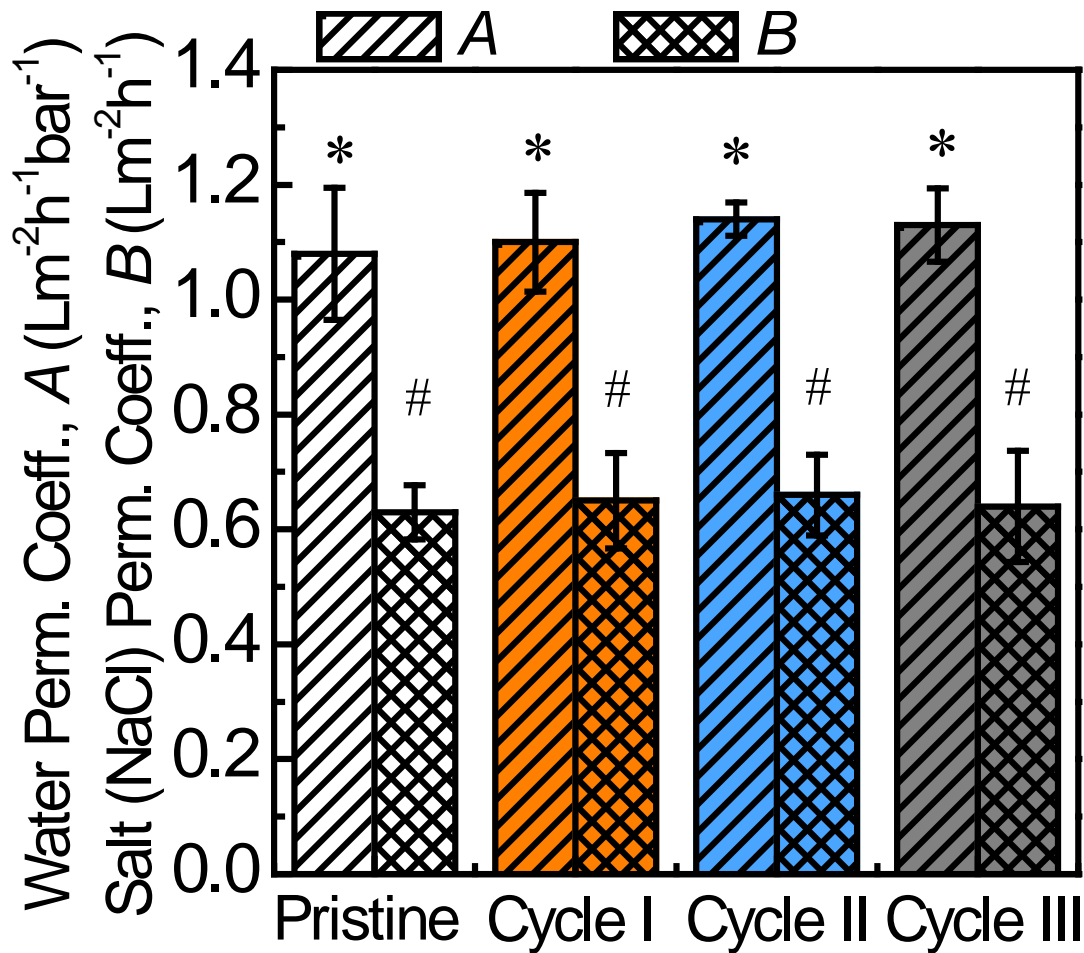
394

395

396

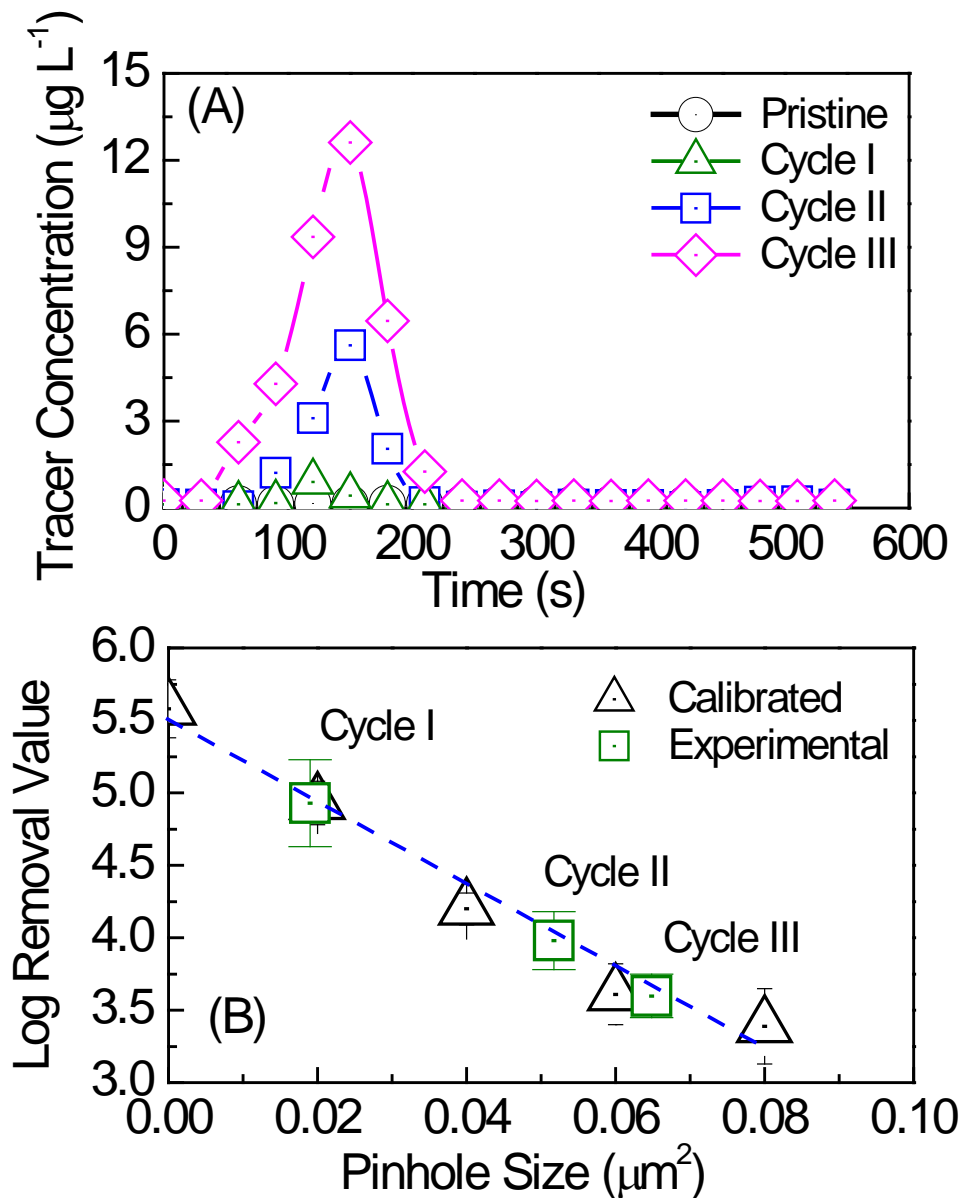
397

Figure 2: SEM micrographs of (A) FO membrane and (C) spacer at the conclusion of gypsum scaling experiments. The potential impaired membrane was revealed in (B) and (D) where a clear indent of spacer was observed.

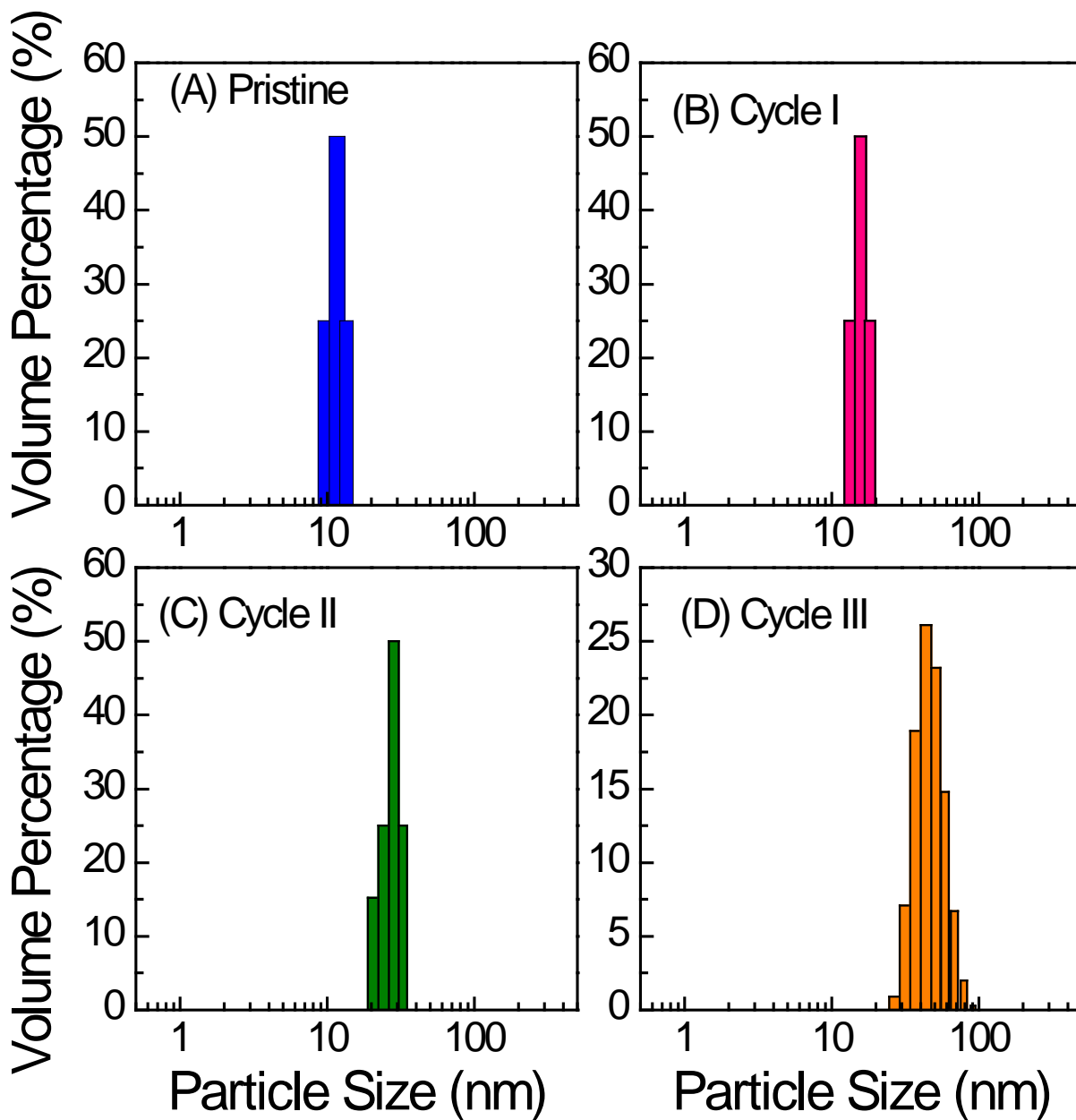


398

399 **Figure 3:** Water and salt (NaCl) permeabilities of pristine membrane and membrane at the
 400 conclusion of each scaling-cleaning cycle. These two key membrane transport parameters were
 401 measured *in situ* using a four-step method in a single FO experiment. The NaCl draw solution
 402 concentration in each step was 0.2, 0.4, 0.7, and 1.2 M. Asterisk and hash symbols above the bar
 403 indicates measurement differences were statistically insignificant (student *t*-test, *p* value>0.05).



404
 405 **Figure 4:** Membrane integrity challenge test using fluorescent Rhodamine WT tracer. (A)
 406 Rhodamine WT concentration in the draw solution as a function of time (B) correlation Log
 407 Removal Value (LRV) with membrane pinhole size. Black triangular symbols represent
 408 membrane LRV obtained from artificial membrane pinhole; the green square symbols were LRV
 409 of membrane at the conclusion of each scaling-cleaning cycle; the blue dotted line was drawn to
 410 guide the eye. Experimental conditions were: the FO membrane cell was operated in one-pass
 411 mode where fluorescent Rhodamine WT solution of 50 mg/L was injected into the FO feeding
 412 tube for 60 seconds at a crossflow rate of 1 L/min. At the same time, the draw solution at the
 413 crossflow rate of 1 L/min was sampled every 10 seconds for a total of 540 seconds.



414

415 **Figure 5:** Membrane integrity challenge test using amine-modified latex nanoparticles. Particle
 416 size distribution of draw solution using (A) pristine membrane, and (B)-(D) membrane at the
 417 conclusion of each scaling-cleaning cycle. The particle size distribution was determined by
 418 dynamic light scattering. Experimental conditions were: the FO membrane cell was operated in
 419 single-pass mode where amine-modified latex nanoparticle solution of 20 mg/L was injected into
 420 the FO feeding tube for 60 seconds at a crossflow rate of 1 L/min. At the same time, the draw
 421 solution at a crossflow rate of 1 L/min was sampled for a total of 540 seconds.